Structure, Vol. 11, 1087–1095, September, 2003, ©2003 Elsevier Science Ltd. All rights reserved. DOI 10.1016/S0969-2126(03)00166-7

Human Brain Neuroglobin Structure Reveals a Distinct Mode of Controlling Oxygen Affinity

Alessandra Pesce,[1] Sylvia Dewilde,[2] Marco Nardini,[1] Luc Moens,[2] Paolo Ascenzi,[3] Thomas Hankeln,[4] Thorsten Burmester,[5] and Martino Bolognesi[1,6,*]

[1]Department of Physics—INFM and Centre for Excellence in Biomedical Research
University of Genova
Via Dodecaneso 33
I-16146 Genova
Italy

[2]Department of Biomedical Sciences
University of Antwerp
Universiteitsplein 1
B-2610 Antwerp
Belgium

[3]Department of Biology
University 'Roma Tre'
Viale Guglielmo Marconi 446
I-00146 Roma
Italy

[4]Institute of Molecular Genetics
Johannes Gutenberg University of Mainz
Becherweg 32
D-55099 Mainz
Germany

[5]Institute of Zoology
Johannes Gutenberg University of Mainz
Müllerweg 6
D-55099 Mainz
Germany

[6]Structural Biology Unit
National Institute for Cancer Research
Largo Rosanna Benzi 10
I-16132 Genova
Italy

Summary

Neuroglobin, mainly expressed in vertebrate brain and retina, is a recently identified member of the globin superfamily. Augmenting O_2 supply, neuroglobin promotes survival of neurons upon hypoxic injury, potentially limiting brain damage. In the absence of exogenous ligands, neuroglobin displays a hexacoordinated heme. O_2 and CO bind to the heme iron, displacing the endogenous HisE7 heme distal ligand. Hexacoordinated human neuroglobin displays a classical globin fold adapted to host the reversible bis-histidyl heme complex and an elongated protein matrix cavity, held to facilitate O_2 diffusion to the heme. The neuroglobin structure suggests that the classical globin fold is endowed with striking adaptability, indicating that hemoglobin and myoglobin are just two examples within a wide and functionally diversified protein homology superfamily.

*Correspondence: bolognes@fisica.unige.it

Introduction

Globins are small respiratory proteins that reversibly bind O_2 by means of an iron-containing porphyrin ring. Globin-like proteins have been identified in bacteria, plants, fungi, and animals (Hardison, 1996, 1998). Most globins are held to sustain O_2 supply to the aerobic metabolism of the respiratory chain (Wittenberg, 1992; Brunori, 1999; Weber and Vinogradov, 2001; Merx et al., 2002), although they have also been ascribed enzymatic functions (Minning et al., 1999; Brunori, 2001; Flögel et al., 2001). In man and other vertebrates, red blood cell hemoglobin (Hb) transports O_2 in the circulatory system. Myoglobin (Mb), typically found in the cardiac and striated muscles, facilitates O_2 diffusion and NO detoxification (Wittenberg, 1970; Perutz, 1979, 1990; Wittenberg and Wittenberg, 1989; Hardison, 1996, 1998; Brunori, 1999; 2001; Flögel et al., 2001). Neuroglobin (Ngb) has recently been identified in the vertebrate nervous system (Burmester et al., 2000; Trent et al., 2001). Furthermore, cytoglobin (Cygb) has been discovered through genomic searches as a fourth globin type expressed almost ubiquitously in human tissues (Burmester et al., 2002; Trent and Hargrove, 2002).

Initially identified in mouse and man (Burmester et al., 2000), Ngb has subsequently been recognized also in rat, pufferfish, and zebrafish (Awenius et al., 2001; Zhang et al., 2002), suggesting a widespread distribution among the vertebrate species. Phylogenetic analyses indicate a common ancient evolutionary origin of vertebrate Ngbs and invertebrate nerve globins (Burmester et al., 2000; Pesce et al., 2002a). Comparison of human neuroglobin (NGB) with vertebrate Mb or Hb shows less than 25% amino acid sequence identity (Figure 1), the sequence conservation among Ngbs from different species being much higher than between orthologous Hbs and Mbs (Burmester et al., 2000). The NGB amino acid sequence (Figure 1) fits well into a globin alignment based on the conserved α helices and the structural motifs of the classical globin fold (Holm and Sander, 1993; Bolognesi et al., 1997; Burmester et al., 2000; Awenius et al., 2001; Pesce et al., 2002a).

Ngb is expressed at the micromolar level in the vertebrate central and peripheral nervous systems, as well as in some endocrine tissues (Burmester et al., 2000; Reuss et al., 2002). Particularly high Ngb concentration has been reported in the mammalian retina, one of the highest-oxygen-consuming tissues of the body (Schmidt et al., 2003). The degree of NGB expression appears to vary in different areas of the human brain, where it is thought to act as hypoxia-inducible neuroprotective factor in hypoxic ischemic injury, such as stroke (Burmester et al., 2000; Moens and Dewilde, 2000). In fact, Ngb has been shown to promote the cell survival of a neuronal cell line kept under hypoxic conditions (Sun et al., 2001,

Figure 1. Structure-Based Sequence Alignment of NGB, MB, HB (α and β Chains), CYGB, Rice Nonsymbiotic Hb, and *C. lacteus* Nerve Hb

The top line depicts the span of α helices in MB (blue), with the topological position assignments, as defined within the vertebrate globin fold. Sequence numbering (bottom line) refers to NGB. The heme Fe-coordinating residues HisE7 and HisF8 are marked in yellow, while apolar residues lining the protein matrix cavity in NGB and in CerHb are marked in blue. Residues making contacts with the heme are highlighted by green asterisks.

2003). Although these observations support an important role of Ngb in the supply of O_2 in nervous tissues, other functions, for example, as an O_2-consuming enzyme or an O_2 sensor, are debated (Pesce et al., 2002a).

Spectroscopic studies show that both ferrous deoxygenated and ferric Ngb forms display a hexacoordinated heme, where residues HisF8 and HisE7 are the fifth (proximal) and the sixth (distal) Fe ligands, respectively. O_2 reversibly displaces the endogenous HisE7 heme ligand, leading to oxygenation of Ngb. The O_2 affinity for the pentacoordinated Ngb species is very high. However, because of HisE7/O_2 competition for coordination to the heme Fe atom, the actual O_2 affinity for Ngb is medium (i.e., P_{50} ca. 1 torr), closely similar to that of Mb (Burmester et al., 2000; Dewilde et al., 2001; Pesce et al., 2002a).

To understand the structural bases of NGB function, we present here the three-dimensional structure of NGB in its hexacoordinated ferric form, at 1.95 Å resolution, as the first instance of a hexacoordinated heme protein observed in vertebrates. Our results reveal that a substantially conserved globin fold can support reversible heme hexacoordination through structural flexibility in the NGB region comprised between C and E helices. Additionally, a wide protein core cavity, enclosing part of the heme distal site, may provide a ligand store/diffusion path whose functional role has no counterpart in vertebrate Hbs or Mbs.

Results and Discussion

The Overall Structure of NGB*

The three-dimensional structure of NGB (bearing the Cys46 → Gly, Cys55 → Ser, and Cys120 → Ser mutations for crystallization purposes, NGB*) was solved by MAD methods based on the anomalous signal of the heme iron atom. Diffraction data were collected at three wavelengths at the ID29 ESRF beamline (Grenoble, France; Table 1), with one crystal of the monoclinic form previously described, which displays four NGB* chains per asymmetric unit (Pesce et al., 2002b). Refinement of the crystal structure converged at a general R factor value of 17.8% (R_{free} of 23.3%), for data in the 40.0–1.95 Å resolution range, with ideal stereochemical parameters (Engh and Huber, 1991; Laskowski et al., 1993). The final model contains 4753 protein atoms, 160 ordered solvent atoms, and 7 sulfate anions (Table 1).

The protein fold in each NGB* chain (Figure 2A) conforms to the classical three over three α-helical sandwich of mammalian Mb and Hb (Holm and Sander, 1993; Bolognesi et al., 1997), where the seven/eight α helices building up the globin fold are conventionally labeled, A, B, …, H, according to their sequential order (topological sites are numbered sequentially within each α helix; Perutz, 1979). For a comparison, rmsd values of 1.18–1.43 Å are calculated (over 108 Cα atom pairs) for the four independent NGB* chains, in structural overlays

Table 1. Data Collection and Refinement Statistics for NGB*

MAD Data Collection Statistics				
	Absorption Peak	Inflection Point	Remote	
Wavelength (Å)	1.738	1.740	0.980	
Resolution (Å)	30–2.5	30–2.5	30–2.2	
Mosaicity (°)	1.2	1.2	1.2	
Completeness (%)	98.6 (93.8)[a]	98.8 (93.5)	99.2 (96.4)	
R_{merge} (%)	6.1 (14.5)	8.5 (18.4)	8.9 (15.6)	
Total reflections	65,453	65,352	196,480	
Unique reflections	17,339	17,369	25,803	
Redundancy	3.8 (3.1)	3.8 (3.1)	7.6 (6.2)	
Average I/σ(I)	9 (5)	6 (4)	5 (4)	
High-Resolution Data Collection Statistics				
Wavelength (Å)	0.933			
Resolution limit (Å)	40–1.95			
Mosaicity (°)	0.76			
Completeness (%)	98.5 (97.9)[b]			
R_{merge} (%)	5.5 (22.0)			
Total reflections	92,865			
Unique reflections	35,871			
Redundancy	2.6 (2.5)			
Average I/σ(I)	17 (5)			
Refinement Statistics and Model Quality				
Resolution range (Å)	40–1.95			
Protein nonhydrogen atoms	4,753			
Water molecules	160			
Sulphate ions	7			
R factor/R_{free}[c] (%)	0.178/0.233			
Space group	$P2_1$			
Unit cell (Å)	a = 39.60, b = 94.93, c = 67.56 β = 94.4°			
Rmsd from ideal geometry				
Bond lengths (Å)	0.012			
Bond angles (°)	0.86			
Ramachandran plot[d]				
Most-favored region	94.2 %			
Additional allowed region	5.8 %			
Averaged B factors (Å²)				
NGB*	*A*	*B*	*C*	*D*
Main chain	27	24	25	24
Side chain	32	29	28	29
All water molecules	31			

[a] Outer shell statistics are shown in parentheses. The outer shells are 2.6–2.5 Å for the absorption peak and inflection point and 2.25–2.20 Å for the remote point.
[b] Outer shell statistics (1.98–1.95 Å) are shown in parentheses.
[c] Calculated with 10% of the reflections.
[d] Data produced with the program PROCHECK (Laskowski et al., 1993).

on MB (Figure 2A). For all the chains, the largest structural deviations are observed in their CD-D regions and in the N-terminal half of the heme distal E helices. In particular, the 44–54 CD segments always protrude from the protein core, with deviations >2.0 Å relative to the structurally equivalent region in MB.

The four NGB* molecules present in the crystallographic asymmetric unit display Cα backbone rmsd values in the 0.2–0.7 Å range and are assembled into two separated loose dimers (*A*/*B* and *C*/*D*, respectively). Two of the four independent NGB* molecules (*A* and *D*) display a partly disordered CD-D region (residues 44–48 in molecule *A* and residues 44–54 in molecule *D*, respectively), showing the highest B factors in the whole structure. Since the CD-D region hosts two out of the three Cys residues that have been mutated for crystallization purposes (Cys46 → Gly and Cys55 → Ser), it cannot be excluded that the mutations enhance the conformational disorder of the CD-D tract and its structural deviation from the corresponding region of MB.

In the *B* and *C* NGB* chains, the CD-D region is stabilized by intramolecular contacts to residues Phe(32)B14 and Leu(39)C5 and is fully structured. The mutated residues Gly46 and Ser55 are completely solvent accessible and buried, respectively, in both *B* and *C* NGB* chains (accessible surface areas of about 80 Å² and 2 Å², respectively). The dihedral angles (ϕ, ψ) for Gly46 are (74°, 18°) for chain *B* and (80°, 23°) for chain *C*; for Ser55, they are (−53°, −26°) for chain *B* and (−69°, −28°) for chain *C*. Within each of the proposed dimers, the association interface (about 700 Å²) hosts mostly polar residue to residue interactions (five main chain to side chain or

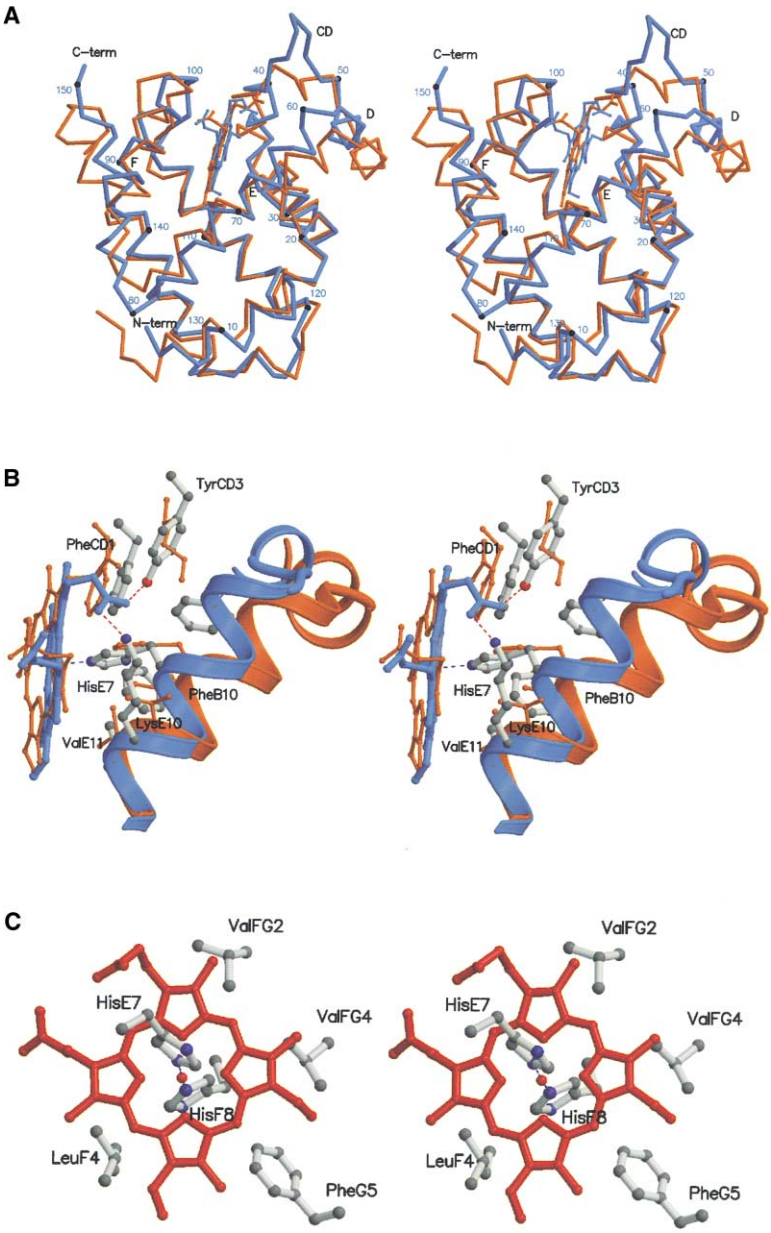

Figure 2. Detailed Views of the NGB* Structure

(A) Stereo view of a Cα trace structural overlay of NGB* (blue, NGB* subunit *C*) on MB (orange). A black sphere is drawn every tenth NGB* Cα atom, together with sequence numbering. In this orientation, the heme is seen edge on, nestled between E and F helices (labeled), with the distal ligand binding site on the right. Notice the conformational differences affecting the CD-D region (labeled), in the top right of the figure.

(B) Stereo view of the heme NGB* distal site region (heme and ribbon, blue; residues, gray), showing the Fe-coordinated HisE7 residue, the PheB10, PheCD1, TyrCD3, LysE10, and ValE11 residues, and the E helix, superimposed on the corresponding residues of MB (orange ribbon and thin bonds). The NGB* coordination bonds between HisE7 and the heme Fe atom are highlighted by a dotted blue line. The two electrostatic/hydrogen bonds stabilizing the heme A propionate are highlighted by dotted red lines.

(C) Stereo view of heme hexacoordination in NGB*. The distal residue HisE7 and the proximal residues LeuF4, HisF8, ValFG2, ValFG4, and PheG5 are shown. Note the close to orthogonal azimuthal orientations of HisE7 and HisF8 imidazole rings. These figures were drawn with MOLSCRIPT (Kraulis, 1991) and Raster3D (Merritt and Bacon, 1997).

side chain to side chain hydrogen bonds and 20 van der Waals contacts), often mediated by a solvent layer built by about 20 water molecules. The association interface, hosting also a sulfate anion, is built by the heme propionates and by residues belonging to helices E and F and to the EF loop of each protomer. In this respect, however, it must be considered that ligand binding studies do not indicate the presence of cooperativity in O_2 binding and that size exclusion chromatography does not provide evidence for the presence of a dimeric species in solution.

Hexacoordination of the Heme Group in NGB*

The NGB* distal site is characterized by a coordination bond connecting the heme Fe atom to the distal His(64)E7 NE2 atom (average value of 2.16 Å for *A* and *B* chains; average value of 2.07 Å for *C* and *D* subunits; see Figures 2B and 2C and Table 2). The HisE7 imidazole ring is almost perfectly staggered relative to the heme pyrrole N atoms, being oriented toward the methinic bridge CHA and CHC atoms of the porphyrin ring. As a result of protein coordination on the heme distal site, the E helix is pulled toward the heme by about 3 Å, relative to MB. The distal site is therefore crowded by the apolar residues Phe(28)B10, Phe(42)CD1, and Val(68)E11 [all falling $<$4.0 Å from His(64)E7], whereas Lys(67)E10 falls outside the heme crevice, being stabilized by electrostatic interaction with the heme propionates (Figure 2B). No polar or low-polarity residues or ordered water molecules are present inside the heme distal pocket. However, the presence of residual electron density for the heme vinyl and methyl substituents indicates the occurrence of substantial heme isomerism in all the four NGB* chains.

Table 2. Heme Coordination Geometry of the Four NGB* Chains Present in the Asymmetric Unit

	A	*B*	*C*	*D*
Average Fe-N(pyrrole) (Å)	2.04	2.03	2.03	2.03
HisE7 NE2-Fe (Å)	2.15	2.17	2.06	2.08
HisF8 NE2-Fe (Å)	2.09	2.02	2.10	2.02
Fe-heme plane deviation (Å)	−0.046	0.047	0.012	0.034
Proximal His(98)F8				
Tilt angle (°)[a]	86	87	83	86
Dihedral NA-Fe-NE2-CE1 (°)	−115	−121	−112	−113
Distal His(64)E7				
Tilt angle (°)	82	82	88	86
Dihedral NA-Fe-NE2-CE1 (°)	−129	−121	−121	−121

[a] The tilt angle lies between the line Fe---HisF8 NE2 (or Fe---HisE7 NE2) atom and the normal to the mean heme plane.

The proximal His(96)F8 residue provides a coordination bond of 2.09 Å for the *A* and *C* subunits and of 2.02 Å for the *B* and *D* subunits to the heme Fe atom, being staggered relative to the heme pyrrole N atoms (see Figure 2C and Table 2). Such a staggered orientation allows the Fe atom to achieve a relaxed position essentially contained in the heme plane, that is, in keeping with a low barrier to ligand binding on the distal site, after HisE7 coordination is removed. Notably, since the His(96)F8 imidazole ring is oriented as a line connecting the heme methinic bridge CHB and CHD atoms, the distal and proximal His imidazoles display approximately orthogonal azimuthal orientations. The His(96)F8 imidazole ring is stabilized by a hydrogen bond between the histidyl ND1 atom and Leu(92)F4 O atom (values ranging between 2.70 Å and 2.76 Å for the four NGB* chains).

Of the known Hb and Mb crystal structures, ferric hemoglobin from the sea cucumber *Caudina arenicola* (Mitchell et al., 1995) shows a hexacoordinated heme in the ligand-free form. Contrary to NGB*, the protein displays a short structured D helix, which disappears when the cyanide ligand is bound. The tetrameric Hb structure from the antarctic fish *Trematomus newnesi* (Riccio et al., 2002) displays two α subunits with a heme Fe-coordinated CO ligand and two β subunits in hexacoordinated form (where HisE7 is the sixth heme Fe ligand). Both CD regions in the β subunits are completely disordered. Remarkably, bis-histidyl heme coordination has also been reported for nonsymbiotic plant Hbs. In particular, the rice nonsymbiotic Hb (165 residues) (Hargrove et al., 2000) displays a hexacoordinated heme in both the ferrous and ferric derivatives, being able to bind O_2 rapidly and with high affinity. A comparison of NGB* and nonsymbiotic rice Hb shows that, in the context of a generally good structural match (rmsd of 1.38 Å, calculated over 104 Cα pairs), both proteins display altered conformation of the CD-D region relative to MB. Unfortunately, however, such a comparison cannot be extended to further details, since the CD-D region conformation in nonsymbiotic rice Hb could only be assigned through molecular modeling (Hargrove et al., 2000).

In a very recent communication, the NMR structure of hexacoordinated ferric *Synechocystis* sp. PC6803 truncated Hb was reported. Although truncated Hbs essentially lack a sizeable CD-D region (Wittenberg et al., 2002), it can be noticed that, even for this Hb case, substantial conformational transitions have been proposed to follow dissociation of the endogenous HisE10 ligand from the heme (Falzone et al., 2002).

The structural properties of NGB* and rice nonsymbiotic Hb and the parallel observations in *C. arenicola* and *T. newensi* Hbs suggest that conformational flexibility of the CD-D regions in globins capable of heme endogenous hexacoordination may have functional roles in relation to the need for displacing the HisE7 ligand upon O_2 binding. The removal of the His(64)E7 imidazole ring from the heme Fe coordination sphere in NGB and the swinging of the histidyl residue out of the distal pocket must overcome conformational barriers related to the close location of the His(64)E7 residue to the porphyrin ring and to cleavage of the Lys(67)E10-heme propionate ion pair. It may then be expected that, in deoxygenated pentacoordinated NGB, the distal E helix shifts away from the heme, leaving room for O_2 diffusion to the heme distal site and stabilization of the heme Fe-bound ligand through a hydrogen bond, as observed in many oxygenated Mbs or Hbs (Bolognesi et al., 1997; Couture et al., 2001; Dewilde et al., 2001). Such a mechanism would imply that structural transition(s) required for removal of the endogenous His(64)E7 ligand reshape the distal site surroundings, promoting O_2 diffusion to the heme, in keeping with the known high affinity of O_2 for the NGB pentacoordinated species. It would also imply that dissociation of the heme Fe-bound O_2 may be slowed down by specific stabilization of the diatomic ligand (likely through hydrogen bonding to HisE7 and aromatic-electrostatic interactions with PheB10 and PheCD1) (Couture et al., 2001; Dewilde et al., 2001). Thus, the observed flexibility at the CD-D globin region may be a structural fingerprint of Hbs exploiting hexacoordination as a mechanism for the control of O_2 diffusion to/from the heme. It may also be one of the structural factors contributing to the pronounced NGB distal pocket conformational heterogeneity, revealed by infrared and nanosecond time-resolved visible spectroscopy (Kriegl et al., 2002).

A Protein Matrix O_2 Diffusion Pathway for NGB*

A large protein matrix cavity (about 120 $Å^3$) is present in the protein region between the heme distal site and the EF interhelical hinge (Figure 3A). The cavity is lined with hydrophobic residues provided by the B, E, G, and H helices (Figure 1). No crystallographic water molecules are defined by electron density within the cavity. In the static crystal structure, the cavity is closed to external solvent by the protein structure comprised between Val(71)E14 and Ala(74)E17, between Leu85 and Tyr88, and by the side chains of Leu(136)H11 and Tyr(137)H12. However, inspection of the intramolecular contacts indicates that, in a dynamic context, it may gain solvent access through side chain fluctuations in the residues listed above. Remarkably, the cavity is easily mapped in all four NGB* chains, if a probe of 1.2 Å radius is used. When a probe of 1.4 Å is adopted, two of the four NGB*

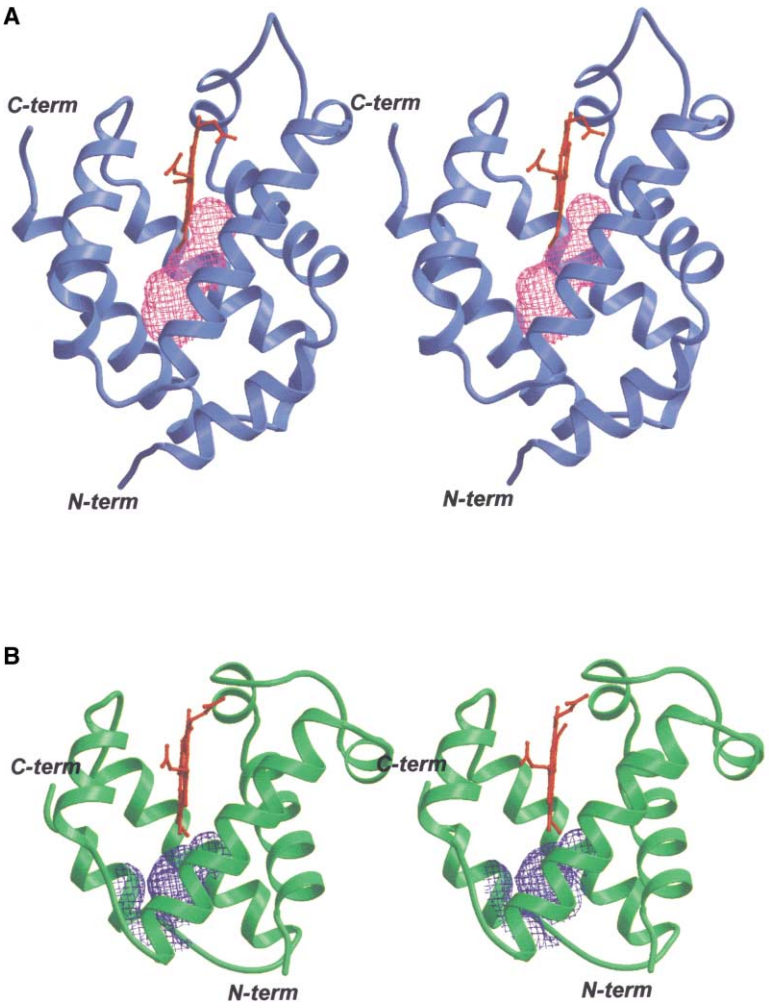

Figure 3. Outline of the Protein Matrix Cavities in NGB* and CerHb

(A) NGB* schematic fold displaying the protein matrix cavity (magenta mesh), which stretches from the heme distal site toward the protein surface.

(B) For comparison, the CerHb three-dimensional structure has been also shown, together with its matrix cavity (blue mesh). The cavity surfaces displayed have been defined by a 1.4 Å radius probe (calculated with the program SURFNET; Laskowski, 1995). This figure was drawn with BOBSCRIPT (Esnousf, 1997).

chains (*A* and *D*) display a narrower cavity (80 Å^3), with an inner neck around residues Ile(72)E15 and Tyr(137)H12, likely a sign of the dynamic spread of the four independent NGB* chain structures observed in the crystal asymmetric unit. Notably, *B* and *C* chains, whose CD-D regions are fully structured, display the wider matrix cavities.

The NGB* protein matrix cavity (Figure 3) is comparable in shape, size, topological location, and the conserved nature of the participating residues (Figure 1) to a protein matrix cavity discovered in the pentacoordinated nerve tissue mini-Hb (the smallest known globin, 109 residues) isolated from the nemertean worm *Cerebratulus lacteus* (CerHb) (Pesce et al., 2002c), held to sustain neural activity during burrowing anoxia conditions. Analysis of the structural database shows that a similarly structured cavity is a unique feature of NGB* and CerHb not shared by Mb, Hb, or hexacoordinate Hbs of known three-dimensional structure. In particular, the NGB* matrix cavity is not comparable to the four smaller cavities found in sperm whale Mb (mapped by Xe binding) (Tilton et al., 1984; Brunori and Gibson, 2001) or to the protein matrix tunnel observed in prokaryotic truncated Hbs (Milani et al., 2001; Wittenberg et al., 2002). Notably, the nonsymbiotic hexacoordinated rice Hb has the corresponding protein matrix region filled by residues Phe(39)B10, Val(77)E11, and Thr(81)E15. The hexacoordinated *Caudina arenicola* Hb has the same core region filled by Met(81)E15 and Phe(117)G8 side chains.

The free energy cost of maintaining a 120 Å^3 cavity within the protein matrix relative to protein stability can be estimated to be in the order of 2–4 kcal/mol (Eriksson et al., 1992). Conservation of a $>$100 Å^3 cavity in NGB* and in the distantly related and much smaller CerHb may therefore indicate its involvement in key functional roles, such as providing a facilitated O_2 diffusion pathway to/from the heme, as an alternative to the distal site gating mechanism based on the HisE7 residue of Hbs and Mbs (Perutz, 1989). Such a ligand diffusion scheme would not contradict the picture proposed above, whereby His(64)E7 coordination to the heme Fe atom is a specific mechanism devised to control the NGB oxygenation process. Alternatively, the NGB* protein matrix cavity may act as a docking/storage station for the ligand during the protein functional cycle, when the heme is in the hexacoordinated state. Both hypotheses would be in keeping with the observation of multiple CO docking sites, among which the ligand can migrate along its pathway to the heme (Kriegl et al., 2002).

Biological Implications

Cytosolic hexacoordinated Hbs are a recent discovery within the Hb protein superfamily. Nevertheless, they have been identified in bacteria, unicellular eukaryotes, plants, some invertebrates, and some vertebrates. This suggests that, rather than being a sporadic evolutionary test, hexacoordinated Hbs may be required to cover essential functions within the cellular metabolism. The structural data presented for NGB* and the ligand binding properties previously reported suggest that heme reversible hexacoordination, via the endogenous HisE7 ligand, may be a simple and effective mechanism for fine-tuning O_2 affinity. A mechanism likely underestimated in the past, since most vertebrate Hb hemichromes (mostly associated with pathological Hb variants) are irreversible (Rifkind et al., 1994), thus not allowing exchange of heme distal ligands. To support reversible hexacoordination structural flexibility of the globin CD-D region, allowing shifting of the E helix to/from the heme distal face, appears to be required.

The new light shed by NGB (and likely by the hexacoordinated Cygb) on structural and functional variation within the Hb homology superfamily adds evidence to the hypothesis that the deeply characterized Hb and Mb are indeed two specialized heme proteins, within a broad evolutionary family, that evolved in (in)vertebrates in response to the demands of circulatory systems and muscles, respectively, thus enabling the onset of larger and more efficient organisms. In this context, other heme proteins (such as Ngb or Cygb) acquired diverse functions, which nevertheless reflect the basic chemical properties of a heme group nestled within a generally well-conserved three over three α-helical sandwich fold. NGB may play a key role in limiting stroke-dependent damage in the brain and protect the retina (a site of intense O_2 consumption) from O_2 deprivation. Insight into NGB structural and functional properties may offer hints for the development of new therapeutics, either enhancing its activity or regulating its cytosolic expression.

Experimental Procedures

Expression, Purification, and Crystallization of NGB*

Expression and purification of NGB* followed the previously described procedure (Dewilde et al., 2001; Pesce et al., 2002b). NGB* was crystallized, at a concentration of 33 mg/ml, from a reservoir solution containing 1.4 M ammonium sulfate, 3% (v/v) isopropanol, and 0.05 M sodium citrate (pH 6.5) at 277 K by the hanging drop vapor diffusion method, as reported elsewhere (Pesce et al., 2002b). Bunches of thin plates grew in about 3–4 weeks, each plate having typical dimensions of $0.3 \times 0.3 \times 0.005$ mm^3. The crystals were stored in a stabilizing solution containing 2.4 M ammonium sulfate, 3% (v/v) isopropanol, and 0.05 M sodium citrate (pH 7.0) at 277 K; they were transferred to the same solution supplemented with 20% (v/v) glycerol immediately prior to data collection.

Data Collection and Processing

A three-wavelength MAD data set was collected at the ESRF synchrotron source (beamline ID29, Grenoble, France) at 100 K (Table 1). The peak and inflection point wavelengths were determined by collecting an X-ray absorption spectrum near the heme iron atom K absorption edge. Moreover, a high-resolution data set (up to 1.95 Å resolution) was collected at the ID14-2 ESRF beamline. Diffraction data were processed with DENZO, SCALEPACK, and programs from the CCP4 suite (CCP4, 1994; Otwinoski and Minor, 1997). The crystals belong to the monoclinic space group $P2_1$, with cell constants of $a = 39.6$ Å, $b = 94.9$ Å, $c = 67.6$ Å, and $\beta = 94.4°$, and accommodate four NGB* molecules per asymmetric unit, with an estimated solvent content of 36% (Table 1).

Structure Solution and Refinement

MAD phases, based on the heme Fe atom anomalous signal, were determined at 2.50 Å resolution with SOLVE (Terwilliger and Berendzen, 1999), with a figure of merit of 0.35. The electron density map was substantially improved by solvent flattening with RESOLVE (Terwillinger, 2000), yielding a figure of merit of 0.58 at 2.50 Å resolution. The resulting electron density map allowed us to almost completely manually trace three out of four NGB* molecules in the asymmetric unit. The molecular model was subsequently improved with the high-resolution data set (1.95 Å resolution) by refinement (REFMAC program; Murshudov et al., 1997) and manual model building (O program; Jones et al., 1991). No use of noncrystallographic symmetry averaging was made throughout the analysis.

The final model contains 580 residues, 160 water molecules, and 7 sulfate anions (R factor = 17.8% and R_{free} = 23.3%, respectively), with ideal stereochemical parameters (Engh and Huber, 1991) (Table 1). No electron density has been observed for amino acids 1, 2, 44–48, 150–151 for chain *A*, amino acids 1–3 for chain *C*, 44–54 and 151 for chain *D*. Weak electron density was observed for part of 10 side chains in chain *A*, 10 side chains in chain *B*, 21 side chains in chain *C*, and 14 side chains in chain *D*, respectively.

Acknowledgments

We would like to thank Dr. Heinz Decker for helpful discussions. This work was supported by grants from the EU Project "Neuroglobin and the Survival of the Neuron" (QLG3-CT-2002-01548), the Italian CNR project "Genomica Funzionale," the ASI (I/R/294/02), and the Deutsche Forschungsgemeinschaft (Bu956/5, Ha2103/3-2). M.B. is grateful to Istituto Giannina Gaslini and CINRO (Genova, Italy) for continuous support. S.D. is a postdoctoral fellow of the FWO (Fund for Scientific Research-Flanders).

Received: March 26, 2003
Accepted: April 12, 2003
Published: September 2, 2003

References

Awenius, C., Hankeln, T., and Burmester, T. (2001). Neuroglobins from the zebrafish *Danio rerio* and the pufferfish *Tetraodon nigroviridis*. Biochem. Biophys. Res. Commun. *287*, 418–421.

Berman, H.M., Westbrook, J., Fenz, Z., Gilliland, G., Bhat, T.N., Weissig, H., Shindyalov, I.N., and Bourne, P.E. (2000). The Protein Data Bank. Nucleic Acids Res. *28*, 235–242.

Bolognesi, M., Bordo, D., Rizzi, M., Tarricone, C., and Ascenzi, P. (1997). Nonvertebrate hemoglobins: structural bases for reactivity. Prog. Biophys. Mol. Biol. *68*, 29–68.

Brunori, M. (1999). Hemoglobin is an honorary enzyme. Trends Biochem. Sci. *24*, 158–161.

Brunori, M. (2001). Nitric oxide moves myoglobin centre stage. Trends Biochem. Sci. *26*, 209–210.

Brunori, M., and Gibson, Q.H. (2001). Cavities and packing defects in the structural dynamics of myoglobin. EMBO Rep. *2*, 674–679.

Burmester, T., Weich, B., Reinhardt, S., and Hankeln, T. (2000). A vertebrate globin expressed in the brain. Nature *407*, 520–523.

Burmester, T., Ebner, B., Weich, B., and Hankeln, T. (2002). Cytoglobin: a novel globin type ubiquitously expressed in vertebrate tissues. Mol. Biol. Evol. *19*, 416–421.

CCP4 (Collaborative Computational Project 4) (1994). The CCP4

suite. Programs for protein crystallography. Acta Crystallogr. D Biol. Crystallogr. *50*, 760–763.

Couture, M., Burmester, T., Hankeln, T., and Rousseau, D.L. (2001). The heme environment of mouse neuroglobin: evidence for the presence of two conformations of the heme pocket. J. Biol. Chem. *276*, 36377–36382.

Dewilde, S., Kiger, L., Burmester, T., Hankeln, T., Baudin-Creuza, V., Aerts, T., Marden, M.C., Caubergs, R., and Moens, L. (2001). Biochemical characterization and ligand binding properties of neuroglobin, a novel member of the globin family. J. Biol. Chem. *276*, 38949–38955.

Engh, R.A., and Huber, R. (1991). Accurate bond and angle parameters for X-ray protein structure refinement. Acta Crystallogr. A *47*, 392–400.

Eriksson, A.E., Baase, W.A., Zhang, X.J., Heinz, D.W., Blaber, M., Baldwin, E.P., and Matthews, B.W. (1992). Response of a protein structure to cavity-creating mutations and its relation to the hydrophobic effect. Science *255*, 178–183.

Esnousf, B.M. (1997). An extensively modified version of MOLSCRIPT that includes greatly enhanced coloring capabilities. J. Mol. Graph. *15*, 138.

Falzone, C.J., Christie Vu, B., Scott, N.L., and Lecomte, J.T.J. (2002). The solution structure of the recombinant hemoglobin from the cyanobacterium *Synechocystis* sp. PCC 6803 in its hemichrome state. J. Mol. Biol. *324*, 1015–1029.

Flögel, U., Merx, M.W., Gödecke, A., Decking, U.K., and Schrader, J. (2001). Myoglobin: a scavenger of bioactive NO. Proc. Natl. Acad. Sci. USA *98*, 735–740.

Hardison, R.C. (1996). A brief history of hemoglobins: plant, animal, protist, and bacteria. Proc. Natl. Acad. Sci. USA *93*, 5675–5679.

Hardison, R.C. (1998). Hemoglobins from bacteria to man: evolution of different patterns of gene expression. J. Exp. Biol. *201*, 1099–1117.

Hargrove, M.S., Brucker, E.A., Stec, B., Sarath, G., Arredondo-Peter, R., Klucas, R.V., Olson, J.S., and Phillips, G.N., Jr. (2000). Crystal structure of a nonsymbiotic plant hemoglobin. Structure *8*, 1005–1014.

Holm, L., and Sander, C. (1993). Structural allignment of globins, phycocyanins and colicin A. FEBS Lett. *315*, 301–306.

Jones, T.A., Zou, J.Y., Cowan, S.W., and Kjeldgaard, M. (1991). Improved methods for building protein models in electron density maps and the location of errors in these models. Acta Crystallogr. A. *47*, 110–119.

Kraulis, P.J. (1991). MOLSCRIPT: a program to produce both detailed and schematic plots of protein structures. J. Appl. Crystallogr. *24*, 946–950.

Kriegl, J.M., Bhattacharyya, A.J., Nienhaus, K., Deng, P., Minkow, O., and Nienhaus, G.U. (2002). Ligand binding and protein dynamics in neuroglobin. Proc. Natl. Acad. Sci. USA *99*, 7992–7997.

Laskowski, R.A. (1995). SURFNET: a program for visualizing molecular surfaces, cavities and intramolecular interactions. J. Mol. Graph. *13*, 323–330.

Laskowski, R.A., MacArthur, M.W., Moss, D.S., and Thornton, J.M. (1993). PROCHECK, a program to check the stereochemical quality of protein structures. J. Appl. Crystallogr. *26*, 283–291.

Merritt, E.A., and Bacon, D.J. (1997). Raster3D: photorealistic molecular graphics. Methods Enzymol. *277*, 505–524.

Merx, M.W., Flögel, U., Stumpe, T., Gödecke, A., Decking, U.K., and Schrader, J. (2002). Myoglobin facilitates oxygen diffusion. FASEB J. *15*, 1077–1079.

Milani, M., Pesce, A., Ouellet, Y., Ascenzi, P., Guertin, M., and Bolognesi, M. (2001). *Mycobacterium tuberculosis* hemoglobin-N displays a protein tunnel suited for O_2 diffusion to the heme. EMBO J. *20*, 3902–3909.

Minning, D.M., Gow, A.J., Bonaventura, J., Braun, R., Dewhirst, M., Goldberg, D.E., and Stamler, J.S. (1999). *Ascaris* haemoglobin is a nitric oxide-activated 'deoxygenase'. Nature *401*, 497–502.

Mitchell, D.T., Barrie Kitto, G., and Hackert, M.L. (1995). Structural analysis of monomeric hemichrome and dimeric cyanomet hemoglobins from *Caudina arenicola*. J. Mol. Biol. *251*, 421–431.

Moens, L., and Dewilde, S. (2000). Globins in the brain. Nature *407*, 461–462.

Murshudov, G.N., Vagin, A.A., and Dodson, E.J. (1997). Refinement of macromolecular structures by the maximum-likeihood method. Acta Crystallogr. D Biol. Crystallogr. *53*, 240–245.

Otwinoski, Z., and Minor, W. (1997). Processing of X-ray diffraction data collected in oscillation mode. Methods Enzymol. *276*, 307–326.

Perutz, M.F. (1979). Regulation of oxygen affinity of hemoglobin: influence of structure of the globin on the heme iron. Annu. Rev. Biochem. *48*, 327–386.

Perutz, M.F. (1989). Myoglobin and hemoglobin: role of distal residues in reactions with haem ligands. Trends Biochem. Sci. *14*, 42–44.

Perutz, M.F. (1990). Mechanisms regulating the reactions of human hemoglobin with oxygen and carbon monoxide. Annu. Rev. Physiol. *52*, 1–25.

Pesce, A., Bolognesi, M., Ascenzi, P., Bocedi, A., Dewilde, S., Moens, L., Hankeln, T., and Burmester, T. (2002a). Neuroglobin and cytoglobin: Fresh blood for the vertebrate globin family. EMBO Rep. *3*, 1146–1151.

Pesce, A., Nardini, M., Dewilde, S., Ascenzi, P., Burmester, T., Hankeln, T., Moens, L., and Bolognesi, M. (2002b). Human neuroglobin: crystals and preliminary X-ray diffraction analysis. Acta Crystallogr. D Biol. Crystallogr. *58*, 1848–1850.

Pesce, A., Nardini, M., Dewilde, S., Geuens, E., Yamauchi, K., Ascenzi, P., Riggs, A.F., Moens, L., and Ascenzi, P. (2002c). The 109-residue nerve tissue mini-hemoglobin from the nemertean worm *Cerebratulus lacteus* highlights striking structural plasticity of the α-helical globin fold. Structure *10*, 725–735.

Reuss, S., Saaler-Reinhardt, S., Weich, B., Wystub, S., Reuss, M., Burmester, T., and Hankeln, T. (2002). Expression analysis of neuroglobin mRNA in rodent tissues. Neuroscience *115*, 645–656.

Riccio, A., Vitagliano, L., Di Prisco, G., Zagari, A., and Mazzarella, L. (2002). The crystal structure of a tetrameric hemoglobin in a partial hemichrome state. Proc. Natl. Acad. Sci. USA *99*, 9801–9806.

Rifkind, J.M., Abugo, O., Levy, A., and Heim, J. (1994). Detection, formation, and relevance of hemichromes and hemochromes. Methods Enzymol. *231*, 449–480.

Schmidt, M., Giessl, A., Laufs, T., Hankeln, T., Wolfrum, U., and Burmester, T. (2003). How does the eye breathe? Evidence for neuroglobin-mediated oxygen supply of the vertebrate retina. J. Biol. Chem. *278*, 1932–1935.

Sun, Y., Jin, K., Mao, X.O., Zhu, Y., and Greenberg, D.A. (2001). Neuroglobin is up-regulated by and protects neurons from hypoxic-ischemic injury. Proc. Natl. Acad. Sci. USA *98*, 15306–15311.

Sun, Y., Jin, K., Peel, A., Mao, X.O., Xie, L., and Greenberg, D.A. (2003). Neuroglobin protects the brain from experimental stroke *in vivo*. Proc. Natl. Acad. Sci. USA *100*, 3497–3500.

Terwillinger, T.C. (2000). Maximum likelihood density modification. Acta Crystallogr. D Biol. Crystallogr. *56*, 965–972.

Terwilliger, T.C., and Berendzen, J. (1999). Automated structure solution for MIR and MAD. Acta Crystallogr. D Biol. Crystallogr. *55*, 849–861.

Tilton, R.F., Jr., Kuntz, I.D., Jr., and Petsko, G.A. (1984). Cavities in proteins: structure of a metmyoglobin-xenon complex solved at 1.9 Å resolution. Biochemistry *23*, 2849–2857.

Trent, J.T., III, and Hargrove, M.S. (2002). A ubiquitously expressed human hexacoordinate hemoglobin. J. Biol. Chem. *277*, 19538–19545.

Trent, J.T., III, Watts, R.A., and Hargrove, M.S. (2001). Human neuroglobin, a hexacoordinate hemoglobin that reversibly binds oxygen. J. Biol. Chem. *276*, 30106–30110.

Weber, R., and Vinogradov, S.N. (2001). Nonvertebrate hemoglobins: functions and molecular adaptations. Physiol. Rev. *81*, 569–628.

Wittenberg, J.B. (1970). Myoglobin-facilitated oxygen diffusion: role of myoglobin in oxygen entry into muscle. Physiol. Rev. *50*, 559–636.

Wittenberg, J.B. (1992). Functions of cytoplasmatic hemoglobins and myohemerythrin. Adv. Comp. Environ. Physiol. *13*, 60–85.

Wittenberg, B.A., and Wittenberg, J.B. (1989). Transport of oxygen in muscle. Annu. Rev. Physiol. *51*, 857–878.

Wittenberg, J.B., Bolognesi, M., Wittenberg, B.A., and Guertin, M. (2002). Truncated hemoglobins: a new family of hemoglobins widely distributed in bacteria, unicellular eukaryotes and plants. J. Biol. Chem. *277*, 871–874.

Zhang, C., Wang, C., Deng, M., Li, L., Wang, H., Fan, M., Xu, W., Meng, F., Qian, L., and He, F. (2002). Full-length cDNA cloning of human neuroglobin and tissue expression of rat neuroglobin. Biochem. Biophys. Res. Commun. *290*, 1411–1419.

Accession Numbers

NGB* atomic coordinates and structure factors have been deposited in the Protein Data Bank (Berman et al., 2000) under accession codes 1oj6 and r1oj6sf, respectively.